PHYSICAL REVIEW E **00**, 000400(R) (2016)

Microscopic treatment of solute trapping and drag

Harith Humadi,[1,2] J. J. Hoyt,[2] and Nikolas Provatas[1]
[1]*Department of Physics, Centre for the Physics of Materials, McGill University, Montreal, QC, Canada*
[2]*Department of Materials Science and Engineering, McMaster University, Hamilton, Ontario*
(Received 3 December 2014; revised manuscript received 3 July 2015; published xxxxxx)

The long wavelength limit of a recent microscopic phase-field crystal (PFC) theory of a binary alloy mixture is used to derive an analytical approximation for the segregation coefficient as a function of the interface velocity, and relate it to the two-point correlation function of the liquid and the thermodynamic properties of solid and liquid phases. Our results offer the first analytical derivation of solute segregation from a microscopic model, and support recent molecular dynamics and numerical PFC simulations. Our results also provide an independent framework, motivated from classical density functional theory, from which to elucidate the fundamental nature of solute drag, which is still highly contested in the literature.

DOI: 10.1103/PhysRevE.00.000400

There are many theories explaining the morphologies and the underlying physics for near-equilibrium systems that evolve towards their equilibrium state [1]. By contrast, theories of physical phenomena associated with far-from-equilibrium systems remain less developed. Rapid solidification from highly undercooled melts serves as a paradigm of such phenomena. In processes like laser-induced surface melting, spray forming, and welding among other technologies, highly supersaturated metastable solid solutions can form. In many cases, the nonequilibrium nature of such process can be exploited to control the degree of supersaturation of the solid. Comprehensive reviews of rapid-solidification technologies that are currently used in the industry along with their theoretical development are offered by [2,3].

At rapid-solidification rates, solute concentration at the solid-liquid interface (SLI) can deviate substantially from the values predicted by the equilibrium phase diagram, a phenomenon known as *solute trapping* [4–10]. In addition to solute trapping, the growth of a crystal with a composition differing from that of its melt requires solute diffusion to move across the SLI. The free-energy dissipation associated by interface diffusion leads to the phenomenon of *solute drag*, an effect which can strongly hinder the transformation rate. Solute drag arises due to a competition between interface diffusion rate and a chemical potential difference across the interface. When the velocity of the SLI is low, local equilibrium is assumed, the chemical potential difference between the SLI essentially vanishes, and solute drag is negligible. As the interface speed increases, solute diffusion limits the rate of partitioning across the interface (solute trapping), leading to an increasing chemical potential jump with velocity and, hence, an increasing solute drag. At large SLI speeds, solute partitioning eventually stops, as does diffusion of solute through the interface, and thus solute drag vanishes.

A phenomenology of solute drag was proposed in the seminal work by Cahn [11] for the case of a grain boundary separating two solid phases. Although the Cahn model quantitatively predicts various aspects of the drag effect, it was assumed that the chemical potential is equal on both sides of the transformation front, an assumption that does not hold for a rapidly solidifying front. Later, Hillert and Sundman [12] incorporated a chemical potential jump into their phenomenology, and proposed that the maximum amount of free energy associated with drag is dissipated. A model for solute drag for solidification was first proposed by Hillert [13], which considered the structure of the interface and its effect on drag. Solute drag experiments are difficult to perform. Some show a significant change in solute concentration at the SLI interface at rapid-solidification rates [14], while some [15] even find no evidence of solute drag. Subsequent models proposed a partial solute drag hypothesis [7,16–18]. More recently, atomistic simulations of Yang *et al.* [17] and Humadi *et al.* [19] proved that the solid-liquid interface stops partitioning solute at a finite velocity, consistent with predictions of Sobolev [9,10] and in contrast to earlier predictions of Aziz *et al.* [5,16].

Traditional phase-field models of solidification consider bulk mass and heat transport coupled to moving interfaces through effective equilibrium boundary conditions [20–27] that map onto traditional sharp interface models. While such an approximation is appropriate at low solidification rates, it is inappropriate at rapid cooling rates where, as described above, nonequilibrium solute partitioning and drag become dominant. Based on the pioneering works of Cahn and Hillert [11–13], modified sharp interface models were developed for rapid solidification [16]. However, these models are typically phenomenological and are based on physically motivated, but often *ad hoc*, parameters that do not link the solidification kinetics to any microscopic quantity of the liquid and solid. More recent phase-field modeling of rapid solidification has shown that phase-field models inherently contain much of the phenomenology of these sharp interface models [7,28]. Still, no fundamental link between the mesoscale solidification process and the microscopic parameters of the materials can be made since solute trapping and drag fundamentally emerge at the atomic scale, where traditional phase-field models, by their very nature, lack any qualitative and quantitative detail [27,29]. At present, no microscopic treatment of the trapping coefficient and solute drag entering rapid-solidification models exists.

Recently, an emerging atomistic continuum modeling formalism coined the *phase-field crystal* (PFC) method has been developed that presents an alternate atomistic framework with which phenomena such as solute trapping can be studied. In contrast to the traditional phase-field approach, PFC models are formulated in terms of order parameters that are periodic at the atomic scale, but whose dynamics evolve over

diffusive time scales relevant to rapid-solidification processes. A phase-field crystal model of binary alloy solidification was first derived in Ref. [30] as a simplification of a truncated density functional theory expanded around the liquid state at coexistence. As such, the model inherits crucial microscopic liquid state parameters originating from the two-point correlation function of the solidifying liquid. The approach has been shown to self-consistently incorporate many physical features of nucleation, multiple crystal orientations, grain boundary energy, elastoplasticity and topological defects and their dynamics [31–38]. In the case of grain growth, Greenwood *et al.* recently simulated grain boundary solute drag using direct simulations of the structural XPFC model [39]. A significant advance in PFC modeling is its use with multiscale and renormalization methods to project out mesoscale phase-field models with complex order parameters [40–42], the coefficients of which maintain their connection to the microscopic liquid and solid state properties inherent in the generating PFC theory. In this work, we use a PFC-derived amplitude model of solidification to elucidate an analytical derivation of the nonequilibrium solute partition coefficient and examine the solute drag associated with solute trapping.

Multiple scale analysis applied to the PFC alloy model in [30] yields the following moving front equations for the impurity concentration (ψ) and the amplitude of the reduced atomic number density (ϕ) [43]:

$$\begin{aligned}\beta V^2\frac{d^2\phi}{dz^2}-V\frac{d\phi}{dz}&=W^2(\hat{n})\frac{d^2\phi}{dz^2}-\frac{\partial f}{\partial\phi},\\ \gamma V^2\frac{d^2\psi}{dz^2}-V\frac{d\psi}{dz}&=\frac{d}{dz}\left(M\frac{d}{dz}\left\{\left(\omega+6B_2^{\ell}\phi^2\right)\psi+u\psi^3\right\}\right).\end{aligned}\tag{1}$$

Their derivation assumes that the atomic number density $n\equiv(\rho-\bar{\rho})/\bar{\rho}$ is represented by $n=n_0+\sum_j A_j e^{iG_j\cdot\vec{x}}$, where n_0 is the reduced average alloy density, and $\bar{\rho}$ is the reference liquid density at coexistence. It is assumed that $n_0=0$ here for simplicity. The $\vec{G}_j$ is the jth reciprocal lattice vector of a general multimode expansion of the density, and A_j is the complex density amplitude corresponding to the jth density wave. We consider here a two-dimensional triangular crystal structure but the qualitative physics of our results are not expected to change for other crystal structures. For solidification, it is suitable to set all the A_j to be real, i.e., $A_j=\phi$. The equations are written in a comoving one-dimensional reference frame moving at velocity V, which is accurate for rapid solidification. The second order derivatives allow for a two-time-scale relaxation of the density and concentration fields. They can be motivated by considering mass and momentum conservation of two-species densities ρ_A and ρ_B [19,34,44]. The coefficients γ and β are microscopic relaxation parameters for the solute and density, respectively, while M is the mobility of impurity atoms. The variable $W(\hat{n})=B_0^x\sum_j\hat{n}\cdot\vec{G}_j$, where $\hat{n}$ is the local interface normal vector and B_0^x is the lowest order coefficient of the solid compressibility. The liquid compressibility is denoted by B^l and expanded as $B^l=B_0^l+B_2^l\psi^2$ [30]. The bulk free energy is denoted by $f(\phi,\psi)$ and $\partial f/\partial\phi=6[\Delta B_0+B_2^l\psi^2]\phi-12t\phi^2+90v\phi^3$, where $\Delta B_0=B_0^l-B_0^x$. The variables t,v,ω,u are the respective coefficients of the bare ϕ^3, ϕ^4, ψ^2, and ψ^4 terms of a Landau expansion of the bulk free energy. Bulk compressibility of the liquid $B^l=1-\bar{\rho}\hat{C}_0$, and $B_0^x=\bar{\rho}(\hat{C})_2^2/(4\hat{C}_4)$, where $\hat{C}_2,\hat{C}_2,\hat{C}_4$ are coefficients of a fourth order expansion of the two-point correlation function of the liquid state, given in Fourier space by $C(\mathbf{k})=\hat{C}_0+\hat{C}_2k^2+\hat{C}_4k^4$ [30]. In what follows, we rescale $\bar{\phi}=\phi/\phi_s$ and $\bar{\psi}=\psi-\psi_s$, where ϕ_s and ψ_s are the bulk order parameter and concentration of the solid phase, respectively. All results presented here are for $\{v,t,u,\omega,B_2^l,B_0^x,W(n),\phi_s,M\}=\{1,0.6,4,0.008,-1.8,1,2,0.06,1\}$.

For the parameters above, the equilibrium partition coefficient of the PFC model of Ref. [30] is $K_e=0.97$. The solidus-to-liquidus jump for this model is $\epsilon=(\psi_s+1)/K_e-(\psi_s+1)\ll 1$, making ϵ an ideal small parameter to expand ψ in due to the high value of K_e in the PFC model. The jump in concentration between liquid and solid is small in most alloy systems and thus we anticipate the results derived below to be applicable in general. Integrating the ψ equation in Eq. (1) from $-\infty$ to z and substituting $\psi\approx\psi_s+\epsilon\psi_1+\epsilon^2\psi_2+\cdots$ into the result gives the following $O(\epsilon)$ equation for ψ_1:

$$\gamma V^2\frac{d\psi_1}{dz}-V\psi_1=M\frac{d}{dz}\left(\left[\omega+6B_2^{\ell}\phi_s^2\phi^2+3u\psi_s^2\right]\psi_1\right).\tag{2}$$

Equation (2) will be used to approximate the concentration profile in the liquid. Higher order terms are needed to approximate concentration in the solid, but that will not be necessary here and will be omitted in what follows.

In Eq. (1) the parameter $W\equiv W(\hat{n})$ is a measure of the SLI width and therefore we approximate the order parameter $\phi\approx\phi_0(z)\equiv[1-\tanh(z/W)]/2$, and define $z=0$, where $\phi_0(0)=1/2$, as the interface between solid and liquid ordering analogous to molecular dynamics studies [17]. $\phi_0(z)$ is the exact lowest order solution of the PFC model for a pure material [45]. We have found that it is also a reasonable approximation for the density amplitude of the PFC alloy model. Substituting the above expression for ϕ into Eq. (2) gives

$$-\frac{V}{M}\psi_1=\frac{d}{dz}\left\{b+\delta\left[1-\tanh\left(\frac{z}{W}\right)\right]^2\right\}\psi_1,\tag{3}$$

where $b\equiv\omega+3u\psi_s^2-\gamma V^2/M$ and $\delta\equiv 6B_2^{\ell}\phi_s^2$. This equation can be solved analytically with an integrating factor that must be solved numerically. In favor of obtaining a tractable analytic expression to work with, we exploit the fact that $\delta/b\sim 10^{-2}$ and $|\tanh|<1$ and seek an analytical solution to lowest order in δ/b. This gives

$$\psi_1\approx e^{-(V/Mb)\{z+(\delta W/b)\Phi_0(z)\}}\{1+O(\delta/b)+\cdots\},\tag{4}$$

where $\Phi_0(z)\equiv\tanh(\frac{z}{W})-2\ln[1+\tanh(\frac{z}{W})]$. In obtaining Eq. (4), the integration constant was found by applying the boundary condition $\psi(z=W/2)=\psi_{\ell}^e\equiv\epsilon+\psi_s$ at $V=0$, where ψ_{ℓ}^e is the equilibrium liquid concentration, and $z=W/2$ defines the point where the concentration profile reaches a maximum, consistent with molecular dynamics [17] and previous PFC alloy simulations [19]. We also take the far field concentration in the liquid to be the same as the solid concentration ψ_s. For simplicity, we analyze only the exponential part of Eq. (4). We found that including the higher order terms gives essentially the same results.

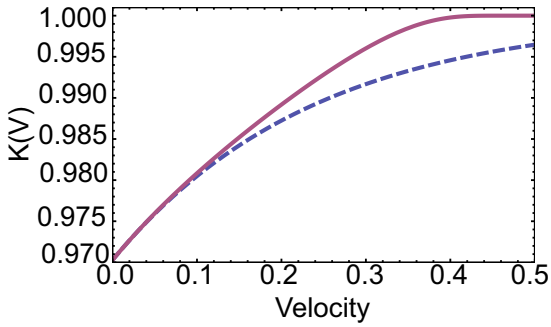

FIG. 1. Segregation coefficient as a function of the interface velocity. The dotted (blue) curve represents the diffusive case where the $K(V)$ tends to unity asymptotically as $V \to \infty$. The solid (purple) curve illustrates the case where the $K(V)$ reaches unity at finite velocity, here $V \approx 0.4$.

Similar formalism was derived for a phase-field model of solidification [46].

The segregation coefficient $K(V)$ is defined to be the ratio of the interface solid concentration to that of the maximum liquid concentration, which occurs when $\phi = 1/2$ at $z = W/2$. In the PFC model, the concentration is expanded around $c = 0.5$, which yields negative concentrations on the left side of the phase diagram. As a result, the solute partition coefficient for the PFC alloy model is defined as

$$K(V) = \frac{\psi_s + 1}{[\psi_s + \epsilon\psi_1(W/2)] + 1}. \tag{5}$$

Figure 1 plots $K(V)$ for two cases: the first case [solid (purple) curve] for $\gamma \neq 0$ and the second case [dotted (blue) curve] for $\gamma = 0$. For the first case, $K(V) = 1$ at a *finite* V, while in the second case, $K(V) \to 1$ only asymptotically as the solid-liquid interface velocity $V \to \infty$.

There are two competing theories for explaining $K(V)$ in the literature. The first, by Aziz [5] assumes purely diffusive solute transport and flux balance across the interface to predict the segregation coefficient. Aziz predicts that $K(V)$ approaches complete trapping [$K(V) = 1$] asymptotically, and never reaches unity at finite V. More recently, Sobolev [9,10] proposed a phenomenology that considered inertial dynamics of solute atoms in the liquid. This led to the emergence of an effective diffusion coefficient, which makes it possible for $K(V)$ to reach unity at a finite velocity.

In our microscopic PFC formalism, the constant b in Eq. (4) emerges as an effective diffusion coefficient. The value of b decreases to zero as the interface velocity increases. As a result, the liquid concentration tends to the solidus concentration. However, this is only true when the relaxation time of the solute diffusion flux is nonzero ($\gamma \neq 0$). Otherwise, b always remains nonzero, and does not change the classical diffusive nature of the concentration profile. This allows for a concentration jump to develop across the two sides of the interface, even for arbitrarily large interface velocities (V).

The above analytical PFC result is consistent with the previous numerical simulations of the alloy PFC model [19] as well as with recent molecular dynamics simulations [17]. We note that a higher order perturbation analysis of the coupled Eqs. (1) would be required to compare the results quantitatively with the full numerical simulations. However, the physics does not change. Our results offer a prediction of the complete solute trapping velocity in terms of microscopic parameters of the PFC theory. Namely, when the constant b defined following Eq. (3) becomes zero, Eq. (4) predicts that ψ_1 will vanish, a consequence of complete trapping. The condition of $b = 0$ occurs when $V^* = \{M(\omega + 3u\psi_s^2)/\gamma\}^{1/2}$, where the approximate form of ψ_s was derived in Ref. [30] as $\psi_s \approx \pm\psi_{sl}(1 + G\{1 - \sqrt{b_{\rm liq}/b_{\rm sol}}\})$, and where the variables in this expression are given by $\psi_{sl} = \sqrt{(\Delta B_0^{sl} - \Delta B_0)/B_2^l}$, $G = -8t^2/\{135v(4\Delta B_0 - 3\Delta B_0^{sl})\}$, $\Delta B_0^{sl} = 8t^2/135v$, while $b_{\rm liq} = (\omega + 3u\psi_{sl})/2$ and $b_{\rm sol} = b_{\rm liq} + 2B_2^l(4\Delta B_0 - 3\Delta B_0^{sl})/5v$. Thus, we have shown that the complete trapping velocity is inversely proportional to the square root of the relaxation time of the solute diffusion flux and proportion to ψ_s, which is determined by the properties of the two-point correlation function of the liquid $C(|\mathbf{k}|)$, through B_l, B_0^x, and the bulk solid free-energy density, through (t, v, ω, u).

Solute drag in the context of the PFC formalism can also be elucidated using Eq. (4). The theoretical formalism of solute drag is briefly summarized here. The free-energy density available for solidification of a binary alloy (denoted here as ΔG_s) is partially dissipated due to solute atoms diffusively redistributing parallel to the solidifying front before attaching to the solid phase. This dissipation is referred to as solute drag, and reduces the total effective free energy available for solidification (denoted here by ΔG_c) to

$$\Delta G_c = \Delta G_s - \Delta G_d, \tag{6}$$

where the maximum drag was shown to be $\Delta G_d = (\psi_\ell - \psi_s)(\mu_\ell - \mu_s)$ [7], while $\Delta G_s = \mathcal{F}_s(\psi_s, T) - \{\mathcal{F}_\ell(\psi_\ell, T) + (\psi_s - \psi_\ell)(\mu_\ell)\}$, derived by Cahn [47], where $\mathcal{F}$ denotes bulk free-energy density and μ_ℓ and μ_s are the interdiffusional chemical potentials of the liquid and solid phase and evaluated at ψ_l and ψ_s, which are, respectively, the liquid and solid concentrations on the liquid and solid sides of the interface. We can equivalently express $\Delta G_s = \psi_s \Delta\mu_B + (1 - \psi_s)\Delta\mu_A$, where $\Delta\mu_A$ ($\Delta\mu_B$) are the solvent A (solute B) chemical potential differences between the solid and liquid phases. Galenko *et al.* [48–50] extended Eq. (6) to include nonequilibrium contributions due to nonzero diffusional flux. They predicted a relation for interface temperature versus velocity that was in excellent agreement with experiments [5,51,52], as well as with numerical results from a study of a two-time PFC alloy model [19]. In what follows, we explore the behavior of the components of Eq. (6) as predicted by amplitude projection of the same PFC alloy model.

The amplitude equations (1) constitute a phase-field theory derived by coarse graining a microscopic PFC model. Analogously to Ref. [7] we thus compute the above expressions for ΔG_s and ΔG_d from the free energy of the PFC amplitude model. This is derived from $f(\phi, \psi)$, which in the bulk gives

$$\mathcal{F}_s = \frac{45v\phi_s^4}{2} - 4t\phi_s^3 + 3\left(B^\ell - B_0^x\right)\phi_s^2 + \frac{u\psi_s^4}{4} + \frac{\omega\psi_s^2}{2},$$
$$\mathcal{F}_\ell = \frac{u\psi_l^4}{4} + \frac{\omega\psi_l^2}{2} \tag{7}$$

for the free-energy density in the solid ($\mathcal{F}_s$) and liquid ($\mathcal{F}_\ell$).

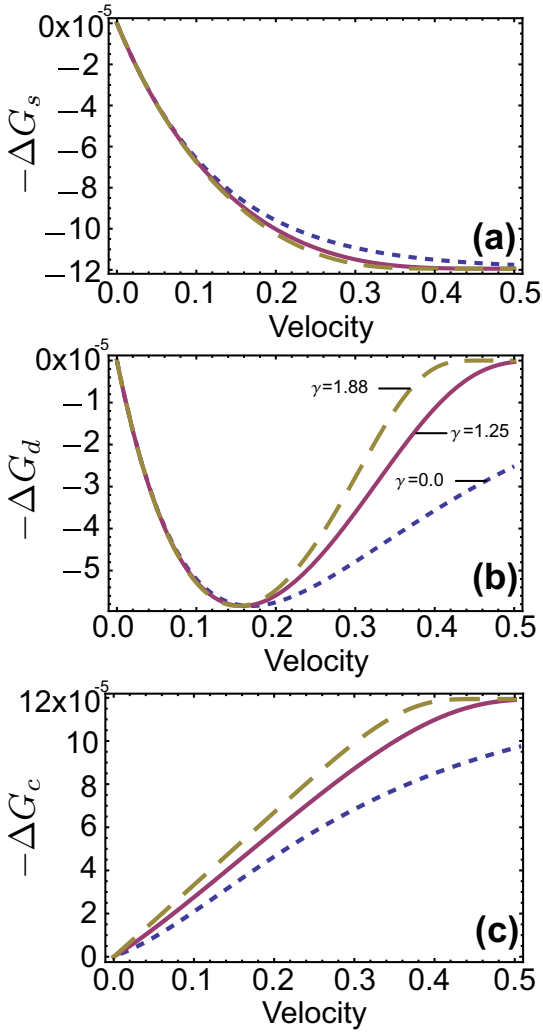

FIG. 2. The driving forces for crystallization for diffusion flux relaxation time coefficients $\gamma = 0, 1.25, 1.88$, where the style (color) corresponding to each γ is shown in panel (b). (a) The total driving force available for transformation. (b) The maximal solute drag. (c) The total available crystallization free energy vs interface velocity.

At low thermodynamic driving forces, molecular dynamics simulations and experiments suggest that $V \propto -\Delta G_c$ [53]. However, this relation becomes less accurate near complete trapping velocities. To study higher velocities, the solid concentration ψ_s and order parameter ϕ_s are assumed constant in the solid during steady-state front propagation, while the liquid concentration $\psi = \psi_s + \epsilon\psi_1$ is determined by Eq. (4). These quantities are substituted into $\mathcal{F}_\ell$ and $\mathcal{F}_s$ to compute ΔG_s, ΔG_c, and ΔG_d. Figure 2(a) shows three different cases of ΔG_s versus V. The dotted blue line represents the diffusive case where the relaxation time for diffusional flux is zero ($\gamma = 0$). The solid (purple) and the dashed (yellow) lines show ΔG_s for $\gamma = 1.24$ and $\gamma = 1.88$, respectively.

Figure 2(b) plots ΔG_d for the same γ values as Fig. 2(a). It is noteworthy that the maximum amount of solute drag (minimum of ΔG_d) does not change as the degree of trapping (γ) changes. However, the curvature of ΔG_d at large V is quite sensitive to γ. This occurs because as γ increases, complete trapping occurs at lower velocity (V^*). This causes the concentration difference across the interface to decrease rapidly for $V > V^*$, thus leading to a decrease in ΔG_d, which depends on $\psi_\ell - \psi_s$. This confirms previous solute drag phenomenologies, and is consistent with recent molecular dynamics results [17]. Our results illustrate that as the solute relaxation coefficient γ changes V^* and the degree of solute trapping, it affects the driving force for complete crystallization mostly through ΔG_d since ΔG_s does not change appreciably with γ for $V > V^*$. Figure 2(c) shows a nearly linear relationship of the driving force with velocity up to above the speed of complete trapping V^*, after which it becomes constant. The slope of this dependence depends on the relaxation time of solute flux, in agreement with the nonequilibrium theory of Galenko in Ref. [48].

Other materials parameters of our phase-field crystal theory were also examined for their effect on solute drag. An important one is the equilibrium solute partition coefficient K_e, which is controlled by ν, the coefficient of the ϕ^3 term in the bulk PFC free-energy functional. Increasing ν leads to increasing K_e. Materials with larger K_e exhibit lower complete trapping velocities (V^*) because less driving force is required to reach complete trapping for a decreasing concentration jump $\psi_\ell - \psi_s$. Thus, solute drag ΔG_d also decreases as K_e increases. Figure 3 illustrates $-\Delta G_c$ vs V for three values of ν (or, equivalently, K_e), at a fixed γ (other parameters are as indicated at the beginning of this Rapid Communication). This illustrates that in all cases, the driving force for crystallization (ΔG_c) increases as solute drag decreases because of the decreasing of ΔG_d. This implies that solute drag is strictly a kinetic process (i.e., ΔG_d depends on V, through K_e). Previous models have attempted to simplify the contribution of solute drag by defining a single adjustable parameter f (Ref. [5,17]), which varies from zero for the no drag limit and unity for maximum drag. The discussion of the f parameter are further discussed in Ref. [43].

In summary, an amplitude model derived from a microscopic phase-field crystal model has been derived to study the phenomena of solute trapping and solute drag, two important materials processes that remain poorly understood. We have derived a first order analytic expression for the concentration profile in the liquid as a function of interface velocity and position, and used it to derive the solute trapping coefficient $K(V)$. Our model predicts that when inertial dynamics

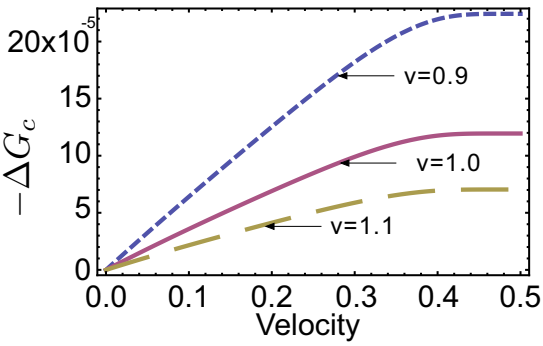

FIG. 3. The driving force for crystallization; the three different lines show the different K_e by changing the value of ν ($\gamma = 1.88$ is fixed).

are included in solute transport, complete trapping occurs at a finite velocity, consistent with the phenomenology of Sobolev [9,10] and recent molecular dynamics (MD) simulations. A key result is the derivation of an expression for the complete trapping velocity as a function of the bulk compressibility of the solid and liquid and the bulk free energy of each phase.

In addition, we used our result for $K(V)$ to elucidate the role of the solute drag coefficient. As V increases, the maximum solute drag decreases proportionately to the complete trapping velocity and solute flux relaxation time. The larger the relaxation time of the solute diffusion flux (γ), the lower the complete trapping velocity and therefore the smaller the amount of solute drag. For fixed γ, the PFC model predicts a linear relationship between interface velocity and the total free energy for crystallization at small velocities, consistent with recent MD simulations. It was found that the total available free energy for solidification and the maximum solute drag are velocity dependent. Model parameters such as those that alter the equilibrium segregation coefficient (K_e) were also examined. It was found that as K_e increases, complete trapping occurs at slower velocities due to lower driving forces required by the system. This also changes the maximum available solute drag of the system. For the discussion of partial solute drag and how it affects the system, we refer the reader to Ref. [43].

The results of this work comprise independent predictions of solute trapping and drag concepts emerging from a continuum theory that is fundamentally derived from a microscopic density functional theory. As a result, the analytical and numerical results presented here can be related to both thermodynamic material properties of the solid and liquid, as well as to the microscopic correlation properties of the melt from which crystallization occurs.

The authors would like to acknowledge the National Science and Engineering Research Council of Canada (NSERC) for the finical support of this work.

[1] J. P. Gollub and J. S. Langer, Rev. Mod. Phys. **71**, S396 (1999).
[2] E. J. Lavernia and T. S. Srivatsan, J. Mater. Sci. **45**, 297 (2010).
[3] D. M. Herlach and D. M. Matson, *Solidification of Containerless Undercooled Melts* (Wiley-VC, Weinheim, 2012).
[4] J. A. Kittl, P. G. Sanders, M. J. Aziz, D. P. Brunco, and M. O. Thompson, Acta Mater. **48**, 4797 (2000).
[5] M. J. Aziz and T. Kaplan, Acta Metall. **36**, 2335 (1988).
[6] P. Galenko and S. Sobolev, Phys. Rev. E **55**, 343 (1997).
[7] N. A. Ahmad, A. A. Wheeler, W. J. Boettinger, and G. B. McFadden, Phys. Rev. E **58**, 3436 (1998).
[8] K. A. Jackson, K. M. Beatty, and K. A. Gudgel, J. Cryst. Growth **271**, 481 (2004).
[9] S. L. Sobolev, Phys. Lett. A **199**, 383 (1995).
[10] S. L. Sobolev, Phys. Rev. E **55**, 6845 (1997).
[11] J. W. Cahn, Acta. Metall. **10**, 789 (1962).
[12] M. Hillert and B. Sundman, Acta Metall. **24**, 731 (1976).
[13] M. Hillert and M. Schalin, Acta Mater. **48**, 461 (2000).
[14] P. Smith and M. J. Aziz, Acta Metall. **42**, 3515 (1994).
[15] J. A. Kittl, M. J. Aziz, D. P. Brunco, and M. O. Thompson, J. Cryst. Growth **148**, 172 (1995).
[16] M. J. Aziz and W. J. Boettinger, Acta Metall. Mater. **42**, 527 (1994).
[17] Y. Yang, H. Humadi, D. Buta, B. B. Laird, D. Sun, J. J. Hoyt, and M. Asta, Phys. Rev. Lett. **107**, 025505 (2011).
[18] J. Agren, Acta Metall. **37**, 181 (1989).
[19] H. Humadi, J. J. Hoyt, and N. Provatas, Phys. Rev. E **87**, 022404 (2013).
[20] G. Caginalp, Phys. Rev. A **39**, 5887 (1989).
[21] G. Caginalp and E. Socolovsky, SIAM J. Sci. Comput. **15**, 106 (1991).
[22] A. Karma and W. J. Rappel, Phys. Rev. E **57**, 4323 (1998).
[23] N. Provatas, N. Goldenfeld, and J. Dantzig, Phys. Rev. Lett. **80**, 3308 (1998).
[24] S. G. Kim, W. T. Kim, and T. Suzuki, Phys. Rev. E **60**, 7186 (1999).
[25] A. Karma, Phys. Rev. Lett **87**, 115701 (2001).
[26] W. Boettinger, J. Warren, C. Beckermann, and A. Karma, Annu. Rev. Mater. Res. **32**, 163 (2002).
[27] B. Echebarria, R. Folch, A. Karma, and M. Plapp, Phys. Rev. E **70**, 061604 (2004).
[28] P. K. Galenko, E. V. Abramova, D. Jou, D. Danilov, V. G. Lebedev, and D. M. Herlach, Phys. Rev. E **84**, 041143 (2011).
[29] N. Provatas and K. Elder, *Phase-Field Methods in Materials Science and Engineering* (Wiley-VCH Verlag GmbH & Co. KGaA, Weinheim, 2010).
[30] K. R. Elder, N. Provatas, J. Berry, P. Stefanovic, and M. Grant, Phys. Rev. B **75**, 064107 (2007).
[31] K. R. Elder, M. Katakowski, M. Haataja, and M. Grant, Phys. Rev. Lett. **88**, 245701 (2002).
[32] K. R. Elder and M. Grant, Phys. Rev. E **70**, 051605 (2004).
[33] J. Berry, M. Grant, and K. R. Elder, Phys. Rev. E **73**, 031609 (2006).
[34] P. Stefanovic, M. Haataja, and N. Provatas, Phys. Rev. Lett. **96**, 225504 (2006).
[35] J. Mellenthin, A. Karma, and M. Plapp, Phys. Rev. B **78**, 184110 (2008).
[36] P. Stefanovic, M. Haataja, and N. Provatas, Phys. Rev. E **80**, 046107 (2009).
[37] L. Gránásy, G. Tegze, G. I. Tóth, and T. Pusztai, Philos. Mag. **91**, 123 (2011).
[38] G. Tegze, G. I. Tóth, and L. Gránásy, Phys. Rev. Lett. **106**, 195502 (2011).
[39] M. Greenwood, C. Sinclair, and M. Millitzer, Acta. Mater. **60**, 5752 (2012).
[40] B. P. Athreya, N. Goldenfeld, and J. A. Dantzig, Phys. Rev. E **74**, 011601 (2006).
[41] B. P. Athreya, N. Goldenfeld, J. A. Dantzig, M. Greenwood, and N. Provatas, Phys. Rev. E **76**, 056706 (2007).
[42] Z.-F. Huang, K. R. Elder, and N. Provatas, Phys. Rev. E **82**, 021605 (2010).

[43] H. Humadi, Ph.D. thesis, McMaster Univeristy, 2013.
[44] S. Majaniemi and M. Grant, Phys. Rev. B **75**, 054301 (2007).
[45] P. K. Galenko, F. I. Sanches, and K. R. Elder, Physica D **308**, 1 (2015).
[46] V. G. Lebedev, E. V. Abramova, D. A. Danilov, and P. K. Galenko, Int. J. Mater. Res. **4**, 473 (2010).
[47] J. C. Baker and J. W. Cahn, in *Solidification* (ASM, Metals Park, OH, 1971), p. 23.
[48] P. Galenko, Phys. Rev. B **65**, 144103 (2002).
[49] P. Galenko, Mater. Sci. Eng., **A375-377**, 493 (2004).
[50] H. Wang, P. K. Galenko, X. Zhang, W. Kuang, F. Liu, and D. M. Herlach, Acta Mater. **90**, 282 (2015).
[51] M. J. Aziz, Appl. Phys. Lett. **43**, 552 (1983).
[52] K. Eckler, D. Herlach, and M. Aziz, Acta Metall. Mater. **42**, 975 (1994).
[53] D. Turnbull, J. Phys. Chem. **66**, 609 (1962).